Monthly Notices
of the
ROYAL ASTRONOMICAL SOCIETY

MNRAS **456,** 3720–3728 (2016) doi:10.1093/mnras/stv2845

Atomic data and density diagnostics for S IV

G. Del Zanna[1]★ and N. R. Badnell[2]

[1]*DAMTP, Centre for Mathematical Sciences, University of Cambridge, Wilberforce Road, Cambridge CB3 0WA, UK*
[2]*Department of Physics, University of Strathclyde, Glasgow G4 0NG, UK*

Accepted 2015 December 2. Received 2015 November 16; in original form 2015 August 27

ABSTRACT

We present a new large-scale *R*-matrix scattering calculation for S IV. We used the intermediate-coupling frame transformation method and applied term energy corrections. Our calculation has a much larger configuration-interaction and close-coupling expansion than previous calculations. Despite that, we find good agreement in the predicted intensities of the decays from the three 3s $3p^2$ ^{4}P levels around 1400 Å, important for density diagnostics. A discrepancy between the observed and predicted intensity of the 1404.8 Å line, which is known to be blended at least with an O IV transition, is still present. Significant differences compared to previous models are found instead for the 1062.7 and 1073.0 Å lines, useful for diagnostics in low-density plasma such as in nebulae. Several other significant differences were also found, concerning the population of the 3s 3p 3d $^4F_{9/2}$ metastable level, and the intensities of several transitions.

Key words: atomic data – techniques: spectroscopic.

1 INTRODUCTION

Lines from S IV are observed in the spectra of a wide range of astrophysical sources, including nebulae, stellar coronae and the Sun. In principle S IV lines provide a way to measure electron densities, in particular from the spin-forbidden $3s^2$ 3p ^{2}P–3s $3p^2$ ^{4}P transitions around 1400 Å (see e.g. Dufton et al. 1982).

By a strange coincidence, the best diagnostic line around 1404.8 Å happens to be blended with one of the best density-diagnostic line for O IV (see e.g. Flower & Nussbaumer 1975; Feldman & Doschek 1979). The S IV and O IV lines around 1400 Å have been used extensively because they are excellent density diagnostics from the point of view that the ratios are basically insensitive to the electron temperature, unlike most ratios from other ions. The drawback of the S IV and O IV lines is that they are normally weak and the ratios do not vary much with densities, hence accurate atomic data and observations are required.

The ratio of the 1062.7 and 1073.0 Å lines has also been suggested as a good density diagnostic for nebulae (Feldman & Doschek 1991).

Over the years, several atomic structure and scattering calculations for the electron impact excitation of S IV by electrons were carried out. These data were used to predict line intensities to be compared to observations. The results were often very unsatisfactory. For example, Cook et al. (1995) found inconsistent densities from S IV and O IV. Several papers have been written on the subject; see e.g. Brage, Judge & Brekke (1996) and references therein.

Similar problems were found in astrophysical plasmas. For example, in the RR Tel spectra observed by the *Hubble Space Telescope* (*HST*) Goddard high-resolution spectrograph and discussed by Harper et al. (1999).

The main problem turned out to be the incorrect atomic data for S IV. Tayal (2000) carried out a Breit–Pauli *R*-matrix calculation considering the following configurations for the configuration-interaction (CI) and close-coupling (CC) expansion: $3s^2$ 3p, $3s^2$ 3d, $3s^2$ 4l (l=s,p,d,f), $3p^3$, 3s 3p 3d and 3s 3p 4s, giving rise to 24 *LS* terms and 52 fine-structure levels. These calculations provided significantly improved collision strengths.

Keenan et al. (2002) used the atomic data calculated by Tayal (2000) and RR Tel observations obtained with the *HST* STIS, to find excellent agreement between observed and predicted line ratios for S IV (and O IV), with the exception of the 1423.8 Å line, that was clearly blended. Keenan et al. (2002) pointed out that this resolved the long-standing problems with S IV, and that the problems with other observations, mostly solar, were due to the fact that spectra with lower resolution were considered. However, the RR Tel densities are in the low-density limit of most line ratios, and having excellent agreement at such low densities does not guarantee that the atomic data are correct also at high densities.

Tayal (2000) collision strengths were introduced in the v.3 of the CHIANTI data base (Dere et al. 2001). Proton excitation data were also included. One problem, however, was the fact that not all the transitions were published by Tayal (2000), and that radiative data from various sources were collected to build the CHIANTI model for this ion. The level population for this ion was therefore somewhat uncertain.

Del Zanna, Landini & Mason (2002) presented observations at high densities where inconsistencies in the 1404.8 Å line were

★E-mail: gd232@cam.ac.uk

Table 1. A selection of important S IV lines.

i–*j*	Levels	*gf* Present	$A_{ji}(s^{-1})$ Present	$A_{ji}(s^{-1})$ T99 CIV3	$A_{ji}(s^{-1})$ H02 CIV3 (a)	$A_{ji}(s^{-1})$ H02 CIV3 (b)	λ(Å)
2–5	$3s^2\ 3p\ ^2P_{3/2}$–$3s\ 3p^2\ ^4P_{5/2}$	7.7×10^{-5}	4.3×10^{4}	3.4×10^{4}	5.1×10^{4}	4.5×10^{4}	1406.06
2–4	$3s^2\ 3p\ ^2P_{3/2}$–$3s\ 3p^2\ ^4P_{3/2}$	2.3×10^{-5}	1.9×10^{4}	1.3×10^{4}	2.2×10^{4}	1.9×10^{4}	1416.93
1–3	$3s^2\ 3p\ ^2P_{1/2}$–$3s\ 3p^2\ ^4P_{1/2}$	3.6×10^{-5}	6.0×10^{4}	4.8×10^{4}	6.4×10^{4}	6.6×10^{4}	1404.85
2–3	$3s^2\ 3p\ ^2P_{3/2}$–$3s\ 3p^2\ ^4P_{1/2}$	2.6×10^{-5}	4.3×10^{4}	3.8×10^{4}	4.7×10^{4}	4.9×10^{4}	1423.88
1–6	$3s^2\ 3p\ ^2P_{1/2}$–$3s\ 3p^2\ ^2D_{3/2}$	8.8×10^{-2}	1.3×10^{8}	1.3×10^{8}	1.5×10^{8}	–	1062.67
2–7	$3s^2\ 3p\ ^2P_{3/2}$–$3s\ 3p^2\ ^2D_{5/2}$	0.15	1.4×10^{8}	1.4×10^{8}	1.6×10^{8}	–	1072.99
2–13	$3s^2\ 3p\ ^2P_{3/2}$–$3s^2\ 4s\ ^2S_{1/2}$	0.35	3.8×10^{9}	3.9×10^{9}	–	–	554.07
1–13	$3s^2\ 3p\ ^2P_{1/2}$–$3s^2\ 4s\ ^2S_{1/2}$	0.17	1.9×10^{9}	1.9×10^{9}	–	–	551.17
6–23	$3s\ 3p^2\ ^2D_{3/2}$–$3s^2\ 4p\ ^2P_{1/2}$	0.55	2.6×10^{9}	2.2×10^{9}	–	–	837.48
6–21	$3s\ 3p^2\ ^2D_{3/2}$–$3p^3\ ^2P_{1/2}$	0.12	5.6×10^{8}	9.2×10^{8}	–	–	852.76

Notes. T99: Tayal (1999) CIV3 calculations. H02: Hibbert et al. (2002) CIV3 calculations. Case (a) refers to the extended orbitals, valence + core–valence correlations, adjusted. Case (b) refers to the most elaborate calculation, with extended orbitals, valence + core–valence + core–core correlations, adjusted.

found, confirming that indeed at high densities the problems were still there. CHIANTI v.3 was used. Possible explanations were the presence of an unidentified blending line (which becomes strong only at high densities), or inaccuracies in the S IV atomic data at high densities.

It is of particular importance to resolve the 1404.8 Å problem now, since the S IV and O IV lines are routinely observed since 2013 by the *Interface Region Imaging Spectrograph* (*IRIS*; De Pontieu et al. 2014) with high temporal, spatial and spectral resolutions.

S IV is an Al-like ion, as Fe XIV. Previous scattering calculations of Fe XIV have clearly shown the limitations of small CI/CC expansions (see Storey, Mason & Young 2000; Liang et al. 2010; Del Zanna et al. 2015c). The first step is therefore to carry out a larger calculation for S IV. The aim of this paper is to present a new scattering calculation based on an improved target, and see how the new model ion affects the main diagnostics for this ion.

2 ATOMIC STRUCTURE

The atomic structure calculations were carried out using the AUTOSTRUCTURE program (Badnell 2011), which originated from the SUPERSTRUCTURE programme (Eissner, Jones & Nussbaumer 1974), and which constructs target wavefunctions using radial wavefunctions calculated in a scaled Thomas–Fermi–Dirac–Amaldi statistical model potential with a set of scaling parameters. The scaling parameters λ_{nl} for the potentials in which the orbital functions are calculated are 1s: 1.450 50; 2s: 1.085 76; 2p: 1.032 83; 3s: 1.083 08; 3p: 1.057 53; 3d: 1.090 29; 4s: 1.095 77; 4p: 1.071 59; 4d: 1.111 60; 4f: 1.379 70. For the CI expansion, we have chosen the set of 29 configurations (up to $n = 4$) $3s^2\ 3p$, $3s\ 3p^2$, $3s^2\ 3d$, $3s^2\ 4l$ (l=s,p,d,f), $3p^3$, $3s\ 3p\ 3d$, $3s\ 3p\ 4l$ (l=s,p,d,f), $3s\ 3d\ 4l$ (l=s,p,d,f), $3s\ 3d^2$, $3p^2\ 3d$, $3p^2\ 4l$ (l=s,p,d,f), $3p\ 3d^2$, $3p\ 3d\ 4l$ (l=s,p,d,f), $3d^3$, giving rise to 298 *LS* terms and 715 fine-structure levels.

An accurate description of spin–orbit mixing between two levels requires their initial term separation to be accurate. This is frequently not the case, so the term energy correction (TEC) method, introduced by Zeippen, Seaton & Morton (1977) and Nussbaumer & Storey (1978), was used to improve the term separations.

We first reviewed the wavelength measurements and the observed energies as reported by NIST.[1] We focused on the lowest levels, which are the most important ones for diagnostic purposes. We found various small inconsistencies, and revised the experimental level energies E_{exp} obtaining excellent consistency. We also found various incorrect wavelength measurements, especially of the 1404.8 Å line, which are still reported in much of the literature. Details of the revised experimental level energies are given in the appendix.

We then obtained a set of 'best-guess' energies E_{best} by linear interpolation. We then used the E_{best} values to obtain the TEC values, then rerun AUTOSTRUCTURE to obtain the corrected target energies E_{TEC}. The list of the lowest levels is provided in Table A1. We note that the ordering of some of the levels changes once the TEC are introduced. The E_{TEC} energies are very close to the experimental values, so were used to calculate the radiative data, still with AUTOSTRUCTURE. The *A*-values are very close (within about 10 per cent) to those previously calculated by Hibbert, Brage & Fleming (2002), as shown in Table 1. Larger differences with the values calculated by Tayal (1999) are found in some cases.

3 SCATTERING CALCULATION

For the CC expansion, we have retained the lowest 418 levels originating from 175 *LS* terms, to include all the terms of the $3p\ 3d^2$ configuration. This represents a significant improvement over the previous calculations by Tayal (2000), where only 24 *LS* terms were included.

The *R*-matrix method used in the scattering calculation is described in Hummer et al. (1993) and Berrington, Eissner & Norrington (1995). We performed the calculation in the inner region in *LS* coupling and included mass and Darwin relativistic energy corrections.

The outer region calculation used the intermediate-coupling frame transformation method (ICFT) described by Griffin, Badnell & Pindzola (1998). The ICFT method determines the multichannel quantum defect theory (MQDT) unphysical (i.e. largely energy independent) *LS*-coupling reactance matrix and transforms it to intermediate coupling using term coupling coefficients, i.e. it

[1] http://physics.nist.gov

allows for spin–orbit mixing within the target but neglects it for the colliding electron. On using the MQDT expression to transform to the level-resolved physical reactance matrix the closing-off of the unphysical channels gives rise to Rydberg series of resonances converging on the non-degenerate energy levels, as characterized by the $\tan(\pi\nu_j)$ factor. This is discussed in section 2 of Griffin et al. (1998). We used 22 continuum basis functions per orbital to expand the scattered electron partial wavefunction within the *R*-matrix box. This enabled us to calculate converged collision strengths up to 9 Ryd.

We included exchange up to a total angular momentum quantum number $J = 28/2$. We have supplemented the exchange contributions with a non-exchange calculation extending to $J = 76/2$. The outer region part of the exchange calculation was performed in a number of stages. The resonance region was calculated with an energy resolution of 0.000 78 Ryd (Tayal 2000 used a resolution of 0.001 Ryd). A coarse energy mesh was chosen above all resonances.

Dipole-allowed transitions were topped-up to infinite partial wave using an intermediate-coupling version of the Coulomb–Bethe method as described by Burgess (1974) while non-dipole allowed transitions were topped-up assuming that the collision strengths form a geometric progression in *J* (see Badnell & Griffin 2001).

The TECs have been incorporated into the ICFT method as described in Del Zanna & Badnell (2014). The collision strengths were extended to high energies by interpolation using the appropriate high-energy limits in the Burgess & Tully (1992) scaled domain. The high-energy limits were calculated with AUTOSTRUCTURE for both optically allowed (see Burgess, Chidichimo & Tully 1997) and non-dipole allowed transitions (see Chidichimo, Badnell & Tully 2003). The temperature-dependent effective collisions strength $\Upsilon(i - j)$ were calculated by assuming a Maxwellian electron distribution and linear integration with the final energy of the colliding electron. The full data set is made available at our APAP website[2] and will be made available in the future version of the CHIANTI[3] data base (Dere et al. 1997; Del Zanna et al. 2015b).

Fig. 1 shows a comparison with the values calculated by Tayal (2000) at two temperatures, for transitions from the lowest five levels. There is a large scatter, but for most transitions there is agreement within 20 per cent at high temperatures. There is an enhancement in our collision strengths at lower temperatures, which is normally present when the calculation has a large CC expansion, hence more resonance enhancement. There are, however, several transitions for which large discrepancies are present. We have often found that a larger CI expansion can change considerably the oscillator strengths and collision strengths to the higher levels of a smaller calculation (see e.g. Fernández-Menchero, Del Zanna & Badnell 2015), so we would expect the large discrepancies to be associated to the last few levels in Tayal (2000) calculation. However, this is not the case, as we show below. We note also that not all transitions that show these discrepancies are relevant for astrophysical applications.

To find out which collision strengths are important for astrophysical applications, we have calculated the level populations using the collisions strengths and *A*-values. They are shown in Fig. 2. There are clear discrepancies in the population of the metastable 3s 3p 3d $^4F_{9/2}$ level. It turns out that this metastable level provides population to several higher levels which were not included in the 52-level

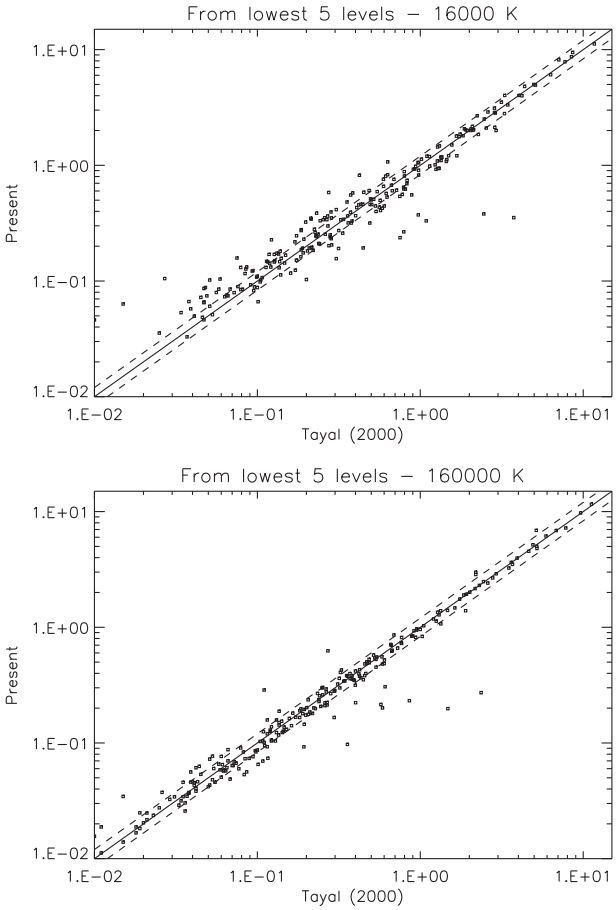

Figure 1. Thermally averaged collision strengths (Tayal 2000 versus the present ones) for transitions from the lowest five levels only at two different temperatures. Dashed lines indicate ± 20 per cent.

CHIANTI model that was based on Tayal (2000) collisions strengths. Including all the levels and all the excitation and de-excitation processes lowers significantly the population of the 3s 3p 3d $^4F_{9/2}$ level, and hence slightly affects the populations of the other important 3s $3p^2$ ^4P metastable levels, and of the ground configuration.

The main levels for density diagnostics are the three 3s $3p^2$ ^4P levels, which produce the lines shown in Table 1. These levels are populated by excitations from the lower levels, and also by radiative cascading. We have found general agreement between the excitations of the main populating transitions of the present large-scale calculation and those of Tayal (2000), as shown in Fig. 3, although there is a slight increase, especially towards lower temperatures, due to the extra resonance enhancements of the present CC expansion. The combined effects of the larger model and different populations have minor effects on the diagnostic ratios, as shown in Fig. 4. The differences are significant at high densities for the 1404.8 Å transition, which is the most important diagnostic line. However, these differences become reduced if the Hibbert et al. (2002) *A*-values (case a) are used instead.

The large discrepancies in Fig. 1 are often associated with levels that do not produce strong transitions. However, a few cases are worth pointing out. The other important diagnostic ratio is the 1062.67/1072.99 Å. The excitation from the ground state to the 3s $3p^2$ $^2D_{3/2}$ which produces the 1062.67 Å (1–6) line is significantly different, as shown in Fig. 5 (top-left plot). Our *A*-value for the 1–6 line is close to that one calculated by Tayal (2000), as shown in

[2] www.apap-network.org
[3] www.chiantidatabase.org

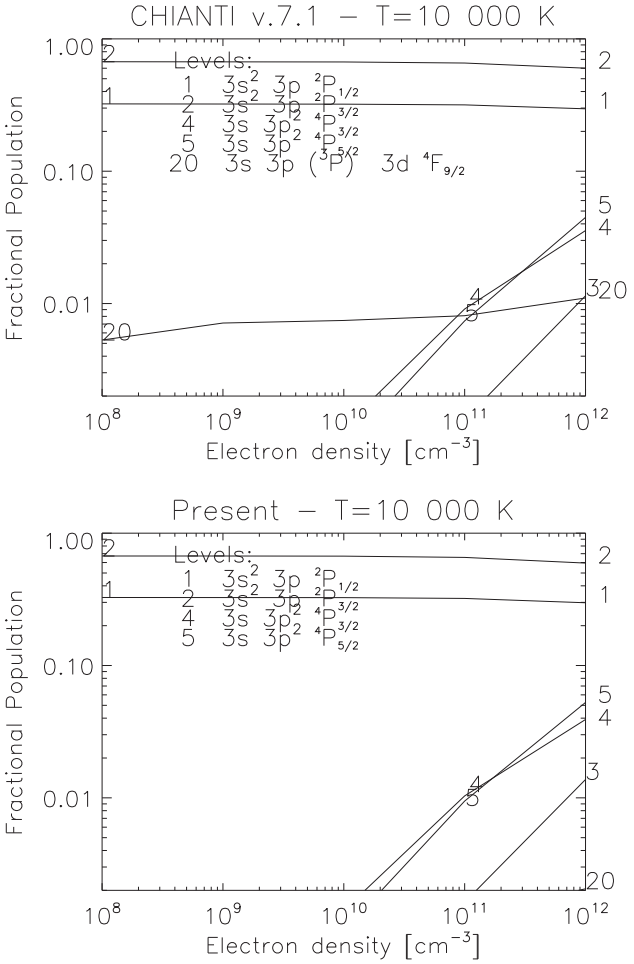

Figure 2. The relative population of the S IV levels, calculated with Tayal's data (as in the CHIANTI data base since v.3) and with the present data.

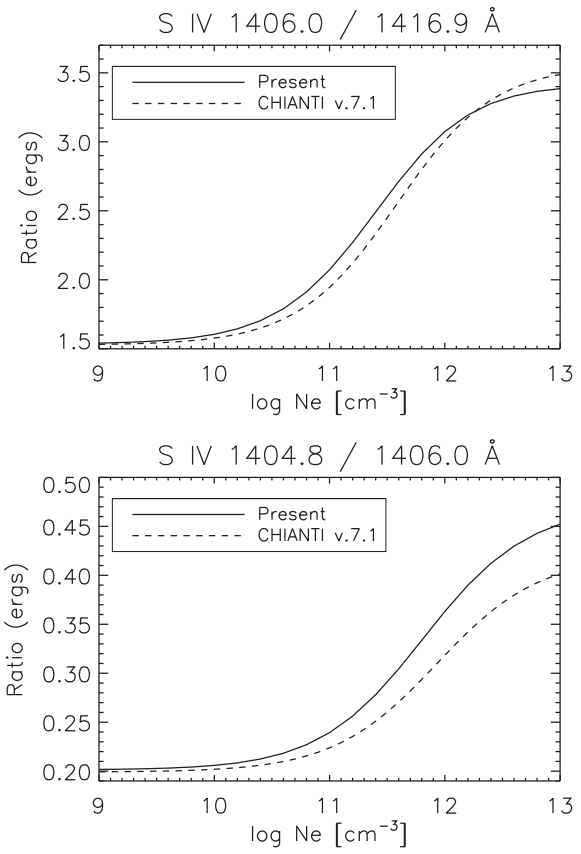

Figure 4. Two of the main density diagnostic ratios around 1400 Å.

Table 1, so the difference is not due to a difference in the atomic structure. Our predicted 1062.67/1072.99 Å ratio, shown in Fig. 6, differs from the previous CHIANTI model.

The decays from the $3s^2\ 4s\ ^2S_{1/2}$ level, at 554 and 551 Å (lines 1–13 and 2–13 in Table 1), are also significantly different, because

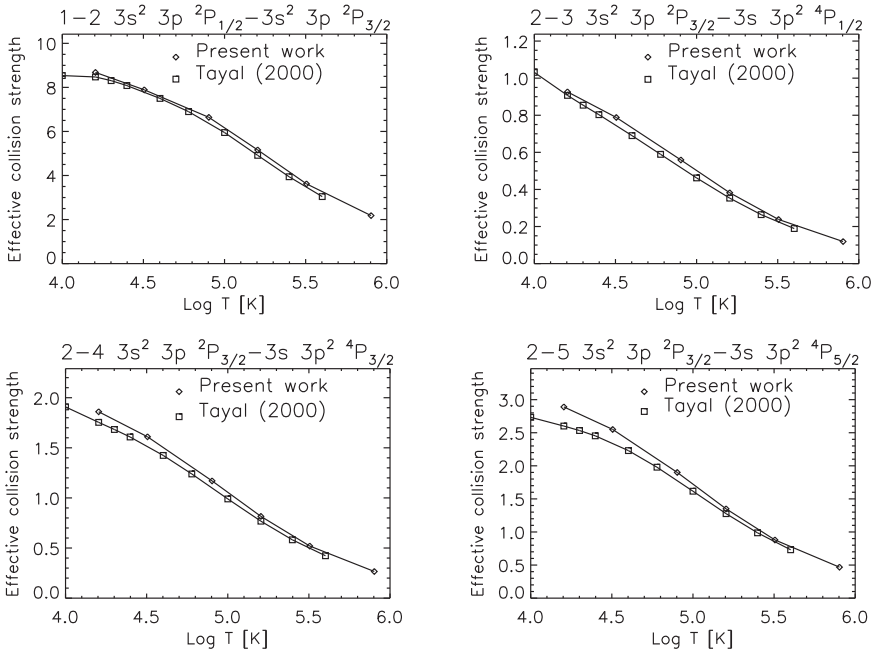

Figure 3. Thermally averaged collision strengths for a selection of transitions compared to those calculated by Tayal (2000).

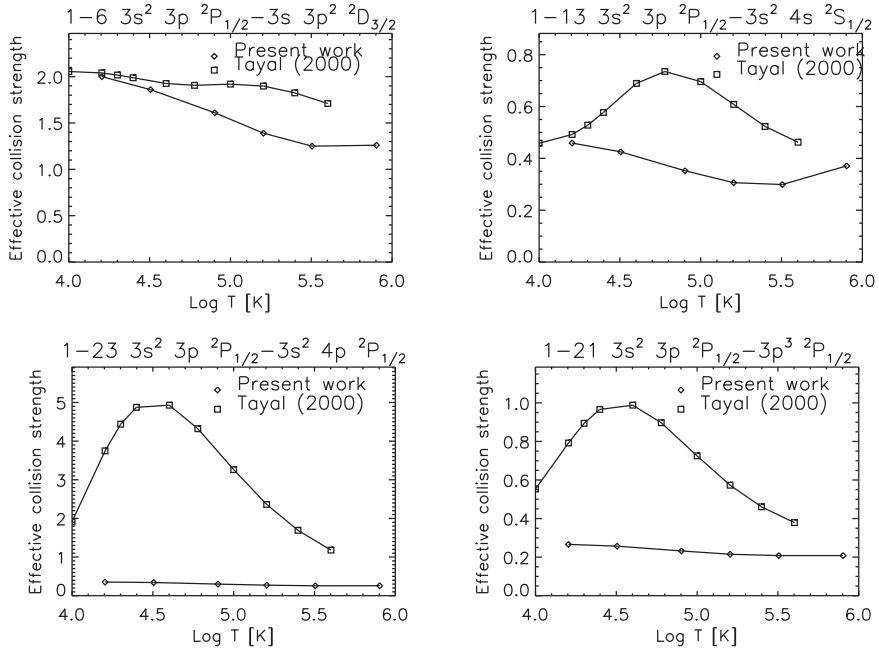

Figure 5. Thermally averaged collision strengths for a selection of transitions compared to those calculated by Tayal (2000).

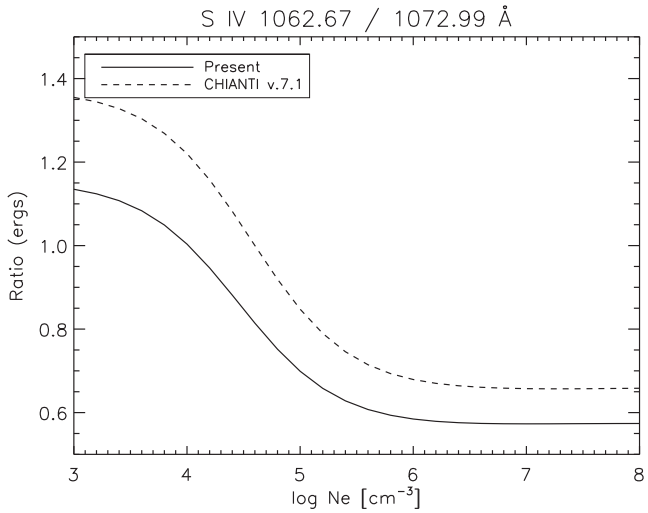

Figure 6. The other main density diagnostic ratio in the UV.

of the different collision strength from the ground state, as shown in Fig. 5 (top-right plot). As in the previous case, our *A*-values are close to those of Tayal.

Finally, the decays of several other levels from the $3s^2$ 4p and $3p^3$ configurations are also significantly different. The most striking case is the 6–23 3s $3p^2$ $^2D_{3/2}$–$3s^2$ 4p $^2P_{1/2}$ transition at 837.48 Å. This transition has been observed in laboratory spectra, but the intensity predicted by our model is almost six times lower than that one calculated with the CHIANTI model. The reason is the large discrepancy in the excitation of the forbidden transition from the ground state, as shown in Fig. 5 (bottom-left plot). Inspection of solar spectra at 837.48 Å clearly indicates that the intensity of this line as predicted by the CHIANTI model is inconsistent with observations.

A similar large discrepancy occurs for the 6–21 3s $3p^2$ $^2D_{3/2}$–$3p^3$ $^2P_{1/2}$, because of the large difference in the excitation from the ground state, as shown in Fig. 5 (bottom-right plot). While the above-mentioned differences are not too large, the differences in the excitation to the $3p^3$ $^2P_{1/2,\,3/2}$ and $3s^2$ 4p $^2P_{1/2,\,3/2}$ levels are large and puzzling. The discrepancies cannot be ascribed to more resonance enhancement (given that our CC expansion is much larger), because our collision strengths are actually smaller than those calculated by Tayal. We have also calculated our collision strengths without the TEC corrections, and found similar results. Finally, our collision strengths are consistent with the high-energy limits calculated with AUTOSTRUCTRUE, so we are confident on the validity of our results.

Table 2. Level energies.

i	Conf.	*LSJ*	E_{T99} Ai	E_{T99} Adj.	E_{T00} Ai	E_{T00} Adj.	E_{exp}
21	$3p^3$	$^2P_{1/2}$	212 012	211 310	213 637	210 882	211 375
22	$3p^3$	$^2P_{3/2}$	212 056	211 420	216 215	212 803	211 363
23	$3s^2$ 4p	$^2P_{1/2}$	213 702	213 439	213 264	213 867	213 513
24	$3s^2$ 4p	$^2P_{3/2}$	213 790	213 593	216 259	213 922	213 724

Notes. Energies in kaysers. E_{T99}: energies from the atomic structure calculation of Tayal (1999), ab initio (Ai) and adjusted (Adj.); E_{T00}: energies from the scattering calculation of Tayal (2000); E_{exp}: present experimental energies.

We have then considered the atomic structure calculation of Tayal (1999), and report in Table 2 the energies of these four levels, obtained with the ab-initio calculation and the one where adjustments to the diagonal elements of the Hamiltonian matrices were applied. We have also compared our *A*-values with those reported by Tayal (1999) and did not find large differences. For example, Table 1 shows the *A*-values for the two main decays from the $3p^3$ $^2P_{1/2}$ and 4p $^2P_{1/2}$ levels. Tayal (1999) obtained 9.2×10^8, 2.2×10^9 while our values are 5.6×10^8, 2.6×10^9, respectively. The other decays have similar differences.

When we looked at the energies in table 1 of Tayal (2000), however, we found two issues. First, the ab initio and adjusted energies of several levels are not the same as those listed in Tayal (1999). This is puzzling, since Tayal (2000) stated to have used the

wavefunctions as described in Tayal (1999). If that was the case, we would have expected that the energies in the two papers were the same. Secondly, the two levels which show the large discrepancies (the $3p^3\ ^2P_{1/2}$ and $4p\ ^2P_{1/2}$ levels) have ab-initio energies in Tayal (2000) that do not follow the experimental ordering, as also shown in Table 2. As described in Table A1, these two levels are highly mixed, so it is possible that Tayal (2000) inverted these two levels. Inverting the ordering of the levels when applying the adjustments to the diagonal elements of the Hamiltonian matrices might be the cause of the large discrepancies.

4 COMPARISON TO OBSERVATIONS

A full discussion of the S IV and O IV diagnostics around 1400 Å is deferred to a future paper. However, we note here that since the present atomic data for S IV are similar to the previous ones for these lines, previous results based on Tayal's cross-sections still hold. At low nebular densities, very good agreement between observed and predicted intensities is found. At high densities, the problem in the S IV and O IV blend at 1404.8 Å discussed in Del Zanna et al. (2002) is still present.

As an example, we have considered the solar observations of an active region by the HRTS second rocket flight in 1978 February, described by Brekke et al. (1991). We have fitted the line intensities trying to remove all the blends, in particular the 1423.8 line which is clearly blended when observed at the excellent HRTS spectral resolution.

We show the comparisons in terms of the 'emissivity ratio' curves (Del Zanna, Berrington & Mason 2004), which are basically the ratios of the observed (I_{ob}, energy units) and the calculated line emissivities as a function of the electron density N_e:

$$R_{ji} = \frac{I_{ob} N_e \lambda_{ji}}{N_j(N_e, T_e)\, A_{ji}}\, C, \qquad (1)$$

where $N_j(N_e, T_e)$ is the population of the upper level j relative to the total number density of the ion, calculated at a fixed temperature T_e. λ_{ji} is the wavelength of the transition, A_{ji} is the spontaneous radiative transition probability and C is a scaling constant that is the same for all the lines within one observation. If agreement between experimental and theoretical intensities is present, all lines should be closely spaced or intersect, for a near isodensity plasma. The value of C is chosen so that the emissivity ratios R_{ji} are near unity where they intersect.

Fig. 7 (top) shows the emissivity ratio curves obtained from the S IV with the present atomic data. The intensities of the 1406.0 and 1416.87 Å indicate a density of about $10^{11.1}$ cm^{-3}, in close agreement with the density obtained from Si III (Del Zanna, Fernández-Menchero & Badnell 2015a). If we adjust the observed intensity of the S IV 1404.8 Å, we then obtain an estimate of the intensity of the O IV 1404.8 Å line.

Fig. 7 (bottom) shows the emissivity ratio curves obtained from the O IV lines. For O IV we have used the CHIANTI v.8 data (Del Zanna et al. 2015b), mainly cross-sections for electron impact excitation from Liang, Badnell & Zhao (2012) and A-values for the lower levels from Corrégé & Hibbert (2004). We note that the proton excitation among the ^4P levels has some effect on the relative intensities of the lines within the multiplet. CHIANTI v.8 includes the proton rates calculated by Foster, Keenan & Reid (1997) using a close-coupled impact-parameter method. The O IV lines indicate a density of about $10^{10.7}$ cm^{-3}, slightly lower than the value one would expect for constant pressure ($10^{10.9}$ cm^{-3}). The estimated intensity of the O IV 1404.8 Å line is still about 30 per cent stronger than predicted.

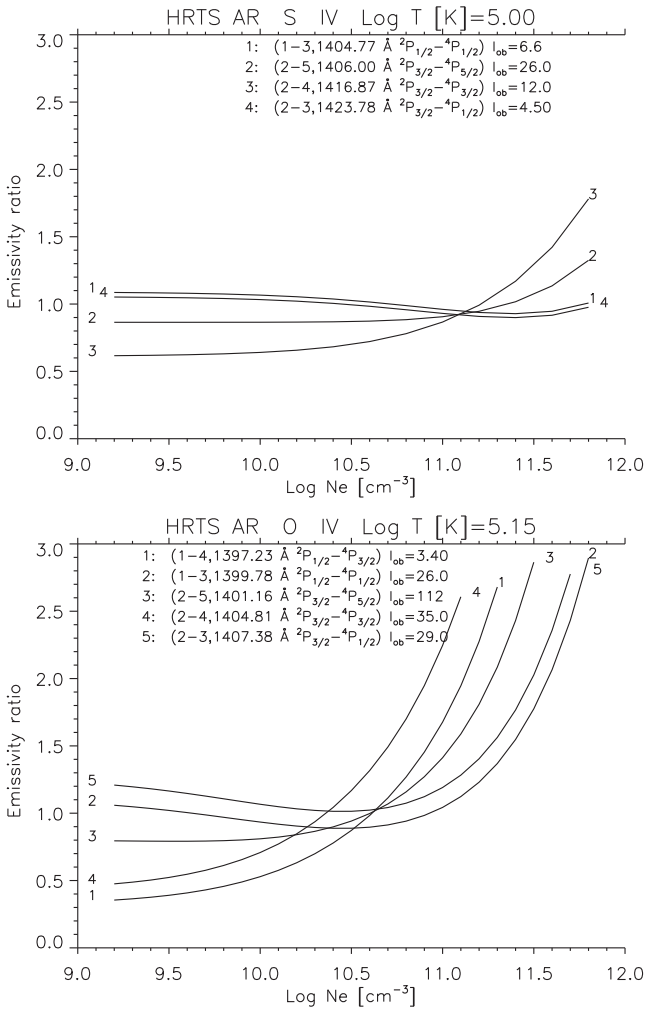

Figure 7. Emissivity ratio curves of the S IV and O IV lines observed during the HRTS second rocket flight on an active region. I_{ob} indicates the observed intensity (erg).

We obtain similar results using stellar UV observations such as those of Capella (Linsky et al. 1995; Del Zanna et al. 2002). The reasons for the discrepancy could well be the presence of an unknown blend. However, the discrepancy is almost within uncertainties, given the marginal density sensitivity of the S IV around 10^{11} cm^{-3}. Another possibility is that proton excitation also affects the S IV ^4P levels. In the literature, we have only found some estimates by Bhatia, Doschek & Feldman (1980) for the rates for proton excitation among two of the ^4P levels. They were obtained using a semi-classical technique (Kastner & Bhatia 1979) and are quite uncertain. Adding these estimates does not affect significantly the populations of the ^4P levels; however, more accurate calculations would be needed before reaching any definitive conclusions.

5 CONCLUSIONS

Despite having run a calculation with much larger CI/CC expansions than Tayal (2000), we have obtained similar populations for the three $3s\ 3p^2\ ^4P$ levels, important for density diagnostics. We confirm that there is still a discrepancy with the important 1404.8 Å line, blend of O IV and S IV. Large problems with the atomic data are now ruled out, so blending with an unknown line is still a possible

explanation. We are currently reviewing *IRIS* observations of several solar flares and active regions to assess if the discrepancy is a common feature.

We found significant differences in the 1062.7 and 1073.0 Å lines, useful for diagnostics in low-density plasma such as in nebulae. We also found an inconsistency in the level population for this ion as calculated within the CHIANTI data base and related to the 3s 3p 3d $^4F_{9/2}$ metastable level.

Several inconsistencies in the collision strengths of other transitions calculated by Tayal (2000) have been found, as shown in Figs 1 and 5. We are confident that our atomic data can reliably be used for astrophysical applications.

ACKNOWLEDGEMENTS

This work was funded by STFC (UK) through the University of Cambridge DAMTP astrophysics grant and the University of Strathclyde UK APAP network grant ST/J000892/1. We would like to thank the anonymous referee for useful comments on the manuscript.

REFERENCES

Badnell N. R., 2011, Comput. Phys. Commun., 182, 1528
Badnell N. R., Griffin D. C., 2001, J. Phys. B: At. Mol. Phys., 34, 681
Berrington K. A., Eissner W. B., Norrington P. H., 1995, Comput. Phys. Commun., 92, 290
Bhatia A. K., Doschek G. A., Feldman U., 1980, A&A, 86, 32
Bowen I. S., 1928, Phys. Rev., 31, 34
Brage T., Judge P. G., Brekke P., 1996, ApJ, 464, 1030
Brekke P., Kjeldseth-Moe O., Bartoe J.-D. F., Brueckner G. E., 1991, ApJS, 75, 1337
Burgess A., 1974, J. Phys. B: At. Mol. Phys., 7, L364
Burgess A., Tully J. A., 1992, A&A, 254, 436
Burgess A., Chidichimo M. C., Tully J. A., 1997, J. Phys. B: At. Mol. Phys., 30, 33
Burton W. M., Ridgeley A., 1970, Sol. Phys., 14, 3
Chidichimo M. C., Badnell N. R., Tully J. A., 2003, A&A, 401, 1177
Cook J. W., Keenan F. P., Dufton P. L., Kingston A. E., Pradhan A. K., Zhang H. L., Doyle J. G., Hayes M. A., 1995, ApJ, 444, 936
Corrégé G., Hibbert A., 2004, At. Data Nucl. Data Tables, 86, 19
De Pontieu B. et al., 2014, Sol. Phys., 289, 2733
Del Zanna G., Badnell N. R., 2014, A&A, 570, A56
Del Zanna G., Landini M., Mason H. E., 2002, A&A, 385, 968
Del Zanna G., Berrington K. A., Mason H. E., 2004, A&A, 422, 731
Del Zanna G., Fernández-Menchero L., Badnell N. R., 2015a, A&A, 574, A99
Del Zanna G., Dere K. P., Young P. R., Landi E., Mason H. E., 2015b, A&A, 582, A56
Del Zanna G., Liang G. Y., Badnell N. R., Fernández-Menchero L., Liang G. Y., Mason H. E., Storey P. J., 2015c, MNRAS, 454, 2909
Dere K. P., Landi E., Mason H. E., Monsignori Fossi B. C., Young P. R., 1997, A&AS, 125, 149
Dere K. P., Landi E., Young P. R., Del Zanna G., 2001, ApJS, 134, 331
Dufton P. L., Hibbert A., Kingston A. E., Doschek G. A., 1982, ApJ, 257, 338
Eissner W., Jones M., Nussbaumer H., 1974, Comput. Phys. Commun., 8, 270
Ekberg J. O., Åke Svensson L., 1970, Phys. Scr., 2, 283
Feldman U., Doschek G. A., 1979, A&A, 79, 357
Feldman U., Doschek G. A., 1991, ApJS, 75, 925
Fernández-Menchero L., Del Zanna G., Badnell N. R., 2015, MNRAS, 450, 4174
Feuchtgruber H. et al., 1997, ApJ, 487, 962
Flower D. R., Nussbaumer H., 1975, A&A, 45, 145
Foster V. J., Keenan F. P., Reid R. H. G., 1997, At. Data Nucl. Data Tables, 67, 99
Griffin D. C., Badnell N. R., Pindzola M. S., 1998, J. Phys. B: At. Mol. Phys., 31, 3713
Harper G. M., Jordan C., Judge P. G., Robinson R. D., Carpenter K. G., Brage T., 1999, MNRAS, 303, L41
Hibbert A., Brage T., Fleming J., 2002, MNRAS, 333, 885
Hummer D. G., Berrington K. A., Eissner W., Pradhan A. K., Saraph H. E., Tully J. A., 1993, A&A, 279, 298
Kastner S. O., Bhatia A. K., 1979, A&A, 71, 211
Kaufman V., Martin W. C., 1993, J. Phys. Chem. Ref. Data, 22, 279
Keenan F. P. et al., 2002, MNRAS, 337, 901
Liang G. Y., Badnell N. R., Crespo López-Urrutia J. R., Baumann T. M., Del Zanna G., Storey P. J., Tawara H., Ullrich J., 2010, ApJS, 190, 322
Liang G. Y., Badnell N. R., Zhao G., 2012, A&A, 547, A87
Linsky J. L., Wood B. E., Judge P., Brown A., Andrulis C., Ayres T. R., 1995, ApJ, 442, 381
Millikan R. A., Bowen I. S., 1925, Phys. Rev., 25, 600
Nussbaumer H., Storey P. J., 1978, A&A, 64, 139
Rank D. M., Holtz J. Z., Geballe T. R., Townes C. H., 1970, ApJ, 161, L185
Sandlin G. D., Bartoe J.-D. F., Brueckner G. E., Tousey R., Vanhoosier M. E., 1986, ApJS, 61, 801
Storey P. J., Mason H. E., Young P. R., 2000, A&AS, 141, 285
Tayal S. S., 1999, J. Phys. B: At. Mol. Phys., 32, 5311
Tayal S. S., 2000, ApJ, 530, 1091
Young P. R., Feldman U., Lobel A., 2011, ApJS, 196, 23
Zeippen C. J., Seaton M. J., Morton D. C., 1977, MNRAS, 181, 527

APPENDIX A: ENERGIES

Table A1 provides a comparison of target level energies. We have slightly revised the energies of several levels and provide new experimental energies E_{exp}. The changes, compared to the NIST values (E_{NIST}) might appear negligible (a few kaysers at most), but are needed to provide accurate wavelength measurements. These are nowadays required, given the high-resolution of current spectrometers such as the *IRIS* mission, to obtain accurate measurements of Doppler shifts.

Only the lowest levels, corresponding to the 52 levels of Tayal's calculation are shown here. We include 69 levels because Tayal did not include the 3s 3p 4p levels. Table A1 also shows the target energies E_t and those obtained with the TEC, E_{TEC}.

Most of the literature values that we adopt for the EUV lines are from Millikan & Bowen (1925) and Bowen (1928). The measurements appear accurate to within a few mÅ. Kaufman & Martin (1993) provided a list of unpublished measurements which had an uncertainty of about 0.02 Å below 2000 Å and 0.03 Å above 2000 Å. The Kaufman & Martin (1993) are generally consistent with those measured by Bowen.

In terms of solar data, the most accurate wavelength measurements in the UV were obtained from several *Skylab* spectra at the limb, as reported by Sandlin et al. (1986). Their accuracy is about 0.005 Å, so we prefer these data over the laboratory measurements.

In principle, accurate measurements for the UV lines could also be obtained from *HST*/STIS spectra of nebulae. However, line profiles are often not symmetric, and discrepancies in the measurements are present. We note that the RR Tel measurements of Young, Feldman & Lobel (2011) are relatively close to the solar ones, but those of Keenan et al. (2002) are incorrect, as already noted by Young et al. (2011), probably because of a problem in the wavelength calibration.

In what follows we provide some details of our revised energies for the lowest levels.

Table A1. Level energies.

i	Conf.	Mixing (per cent)	LSJ	E_{exp}	E_{NIST}	E_{TEC}	E_t
1	$3s^2$ 3p	(94)	$^2P_{1/2}$	0.0	0.0	0.0	0.0
2	$3s^2$ 3p	(94)	$^2P_{3/2}$	951.4	951.4 (0)	918.0 (33)	918.0 (33)
3	3s $3p^2$	(98)	$^4P_{1/2}$	71 182.0	71 184.1 (−2)	71 182.0 (0)	68 963.0 (2219)
4	3s $3p^2$	(98)	$^4P_{3/2}$	71 526.6	71 528.7 (−2)	71 512.0 (15)	69 292.0 (2235)
5	3s $3p^2$	(98)	$^4P_{5/2}$	72 072.2	72 074.4 (−2)	72 042.0 (30)	69 823.0 (2249)
6	3s $3p^2$	(79) +11(c3 17)	$^2D_{3/2}$	94 102.5	94 103.1 (−1)	94 083.0 (20)	94 141.0 (−39)
7	3s $3p^2$	(79) +12(c3 17)	$^2D_{5/2}$	94 148.0	94 150.3 (−2)	94 126.0 (22)	94 183.0 (−35)
8	3s $3p^2$	(96)	$^2S_{1/2}$	123 504.5	123 509.3 (−5)	123 483.0 (22)	126 476.0 (−2972)
9	3s $3p^2$	(93)	$^2P_{1/2}$	133 619.0	133 619.6 (−1)	133 612.0 (7)	136 841.0 (−3222)
10	3s $3p^2$	(93)	$^2P_{3/2}$	134 243.2	134 245.4 (−2)	134 214.0 (29)	137 443.0 (−3200)
11	$3s^2$ 3d	(77) +6(c2 16)	$^2D_{3/2}$	152 128.3	152 133.2 (−5)	152 093.0 (35)	156 489.0 (−4361)
12	$3s^2$ 3d	(77) +7(c2 16)	$^2D_{5/2}$	152 141.3	152 146.8 (−6)	152 127.0 (14)	156 523.0 (−4382)
13	$3s^2$ 4s	(94)	$^2S_{1/2}$	181 432.0	181 448.2 (−16)	181 410.0 (22)	182 750.0 (−1318)
14	$3p^3$	(56) +33(c6 41)	$^2D_{3/2}$	185 055.2	185 055.2 (0)	185 030.0 (25)	183 893.0 (1162)
15	$3p^3$	(56) +32(c6 41)	$^2D_{5/2}$	185 146.7	185 148.0 (−1)	185 128.0 (19)	183 989.0 (1158)
16	$3p^3$	(97)	$^4S_{3/2}$	196 453.7	196 455.4 (−2)	196 431.0 (23)	196 320.0 (134)
17	3s 3p 3d	(98)	$^4F_{3/2}$	203 442.8	203 442.8 (0)	203 427.0 (16)	203 112.0 (331)
18	3s 3p 3d	(98)	$^4F_{5/2}$	203 632.8	203 632.8 (0)	203 617.0 (16)	203 302.0 (331)
19	3s 3p 3d	(98)	$^4F_{7/2}$	203 906.3	203 906.3 (0)	203 886.0 (20)	203 571.0 (335)
20	3s 3p 3d	(98)	$^4F_{9/2}$	204 264.9	204 264.9 (0)	204 236.0 (29)	203 921.0 (344)
21	$3p^3$	(40) +44(c6 15) +23(c7 34)	$^2P_{1/2}$	211 374.8	211 366.6 (8)	211 330.0 (45)	212 904.0 (−1529)
22	$3p^3$	(44) +43(c6 16) +24(c7 28)	$^2P_{3/2}$	211 363.0	211 376.3 (−13)	211 357.0 (6)	212 929.0 (−1566)
23	$3s^2$ 4p	(58) +21(c5 27)	$^2P_{1/2}$	213 513.0	213 514.7 (−2)	213 525.0 (−12)	215 598.0 (−2085)
24	$3s^2$ 4p	(64) +22(c5 23)	$^2P_{3/2}$	213 724.0	213 725.3 (−1)	213 677.0 (47)	215 750.0 (−2026)
25	3s 3p 3d	(96)	$^4P_{5/2}$	222 198.0	222 198.3 (0)	222 191.0 (7)	222 375.0 (−177)
26	3s 3p 3d	(96)	$^4P_{3/2}$	222 487.5	222 488.6 (−1)	222 447.0 (41)	222 631.0 (−144)
27	3s 3p 3d	(97)	$^4P_{1/2}$	222 692.0	222 692.4 (0)	222 624.0 (68)	222 802.0 (−110)
28	3s 3p 3d	(97)	$^4D_{1/2}$	224 339.4	224 342.7 (−3)	224 315.0 (24)	225 004.0 (−665)
29	3s 3p 3d	(96)	$^4D_{3/2}$	224 443.0	224 435.6 (7)	224 406.0 (37)	225 090.0 (−647)
30	3s 3p 3d	(96)	$^4D_{5/2}$	224 537.0	224 539.3 (−2)	224 516.0 (21)	225 199.0 (−662)
31	3s 3p 3d	(98)	$^4D_{7/2}$	224 617.8	224 617.3 (1)	224 612.0 (6)	225 304.0 (−686)
32	3s 3p 3d	(39) +15(c5 23) +52(32)	$^2D_{5/2}$	233 610.4	233 610.4 (0)	233 593.0 (17)	236 149.0 (−2539)
33	3s 3p 3d	(39) +14(c5 23) +51(32)	$^2D_{3/2}$	233 641.7	233 641.7 (0)	233 616.0 (26)	236 173.0 (−2531)
34	3s 3p 3d	(68) +48(28)	$^2F_{5/2}$	241 646.3	241 646.3 (0)	241 645.0 (1)	246 245.0 (−4599)
35	3s 3p 3d	(68) +47(28)	$^2F_{7/2}$	242 421.4	242 421.4 (0)	242 385.0 (36)	246 985.0 (−4564)
36	$3s^2$ 4d	(94)	$^2D_{3/2}$	255 395.8	255 395.8 (0)	255 368.0 (28)	257 421.0 (−2025)
37	$3s^2$ 4d	(94)	$^2D_{5/2}$	255 400.3	255 400.3 (0)	255 383.0 (17)	257 436.0 (−2036)
38	$3s^2$ 4f	(57) +35(c6 15) +47(c6 24)	$^2F_{7/2}$	257 611.0	257 611.0 (0)	257 611.0 (0)	261 963.0 (−4352)
39	$3s^2$ 4f	(57) +34(c6 15) +48(c6 24)	$^2F_{5/2}$	257 742.6	257 742.6 (0)	257 692.0 (51)	262 045.0 (−4302)
40	3s 3p 4s	(98)	$^4P_{1/2}$	263 097.1	263 097.1 (0)	263 171.0 (−74)	263 609.0 (−512)
41	3s 3p 4s	(98)	$^4P_{3/2}$	263 448.1	263 448.1 (0)	263 466.0 (−18)	263 907.0 (−459)
42	3s 3p 4s	(98)	$^4P_{5/2}$	264 067.7	264 067.7 (0)	263 984.0 (84)	264 420.0 (−352)
43	3s 3p 3d	(68) +22(c5 15)	$^2P_{3/2}$	264 882.8	264 882.8 (0)	264 880.0 (3)	270 921.0 (−6038)
44	3s 3p 3d	(67) +21(c5 14) +45(c10 12)	$^2P_{1/2}$	265 055.1	265 055.1 (0)	265 002.0 (53)	271 045.0 (−5990)
45	3s 3p 4s	(83)	$^2P_{1/2}$	270 826.7	270 826.7 (0)	270 897.0 (−70)	275 915.0 (−5088)
46	3s 3p 4s	(85)	$^2P_{3/2}$	271 436.9	271 436.9 (0)	271 372.0 (65)	276 388.0 (−4951)
47	3s 3p 3d	(42) +35(13) +38(c9 38)	$^2F_{7/2}$	277 596.0	277 596.0 (0)	277 561.0 (35)	285 256.0 (−7660)
48	3s 3p 3d	(42) +34(13) +39(c9 37)	$^2F_{5/2}$	277 682.9	277 682.9 (0)	277 680.0 (3)	285 374.0 (−7691)
49	3s 3p 3d	(83)	$^2P_{1/2}$	278 676.9	278 676.9 (0)	278 611.0 (66)	286 990.0 (−8313)
50	3s 3p 3d	(83)	$^2P_{3/2}$	278 642.4	278 642.4 (0)	278 654.0 (−12)	287 024.0 (−8382)
51	3s 3p 3d	(60) +14(c5 15) +33(15)	$^2D_{3/2}$	281 093.6	281 093.6 (0)	281 066.0 (28)	288 385.0 (−7291)
52	3s 3p 3d	(60) +15(c5 15) +32(16)	$^2D_{5/2}$	281 231.6	281 231.6 (0)	281 209.0 (23)	288 520.0 (−7288)
53	3s 3p 4p	(86)	$^2P_{1/2}$	292 569.2	292 569.2 (0)	292 372.0 (197)	293 627.0 (−1058)
54	3s 3p 4p	(90)	$^2P_{3/2}$	292 893.9	292 893.9 (0)	292 620.0 (274)	293 749.0 (−855)
55	3s 3p 4p	(89)	$^4D_{1/2}$	293 310.8	293 310.8 (0)	293 372.0 (−61)	293 042.0 (269)
56	3s 3p 4p	(93)	$^4D_{3/2}$	293 463.1	293 463.1 (0)	293 526.0 (−63)	293 322.0 (141)
57	3s 3p 4p	(98)	$^4D_{5/2}$	293 736.6	293 736.6 (0)	293 811.0 (−74)	293 793.0 (−56)
58	3s 3p 4p	(98)	$^4D_{7/2}$	294 282.2	294 282.2 (0)	294 288.0 (−6)	294 266.0 (16)
59	3s 3p 4p	(97)	$^4P_{1/2}$	297 397.1	297 397.1 (0)	297 427.0 (−30)	300 863.0 (−3466)
60	3s 3p 4p	(96)	$^4P_{3/2}$	297 592.7	297 592.7 (0)	297 591.0 (2)	301 085.0 (−3492)
61	3s 3p 4p	(97)	$^4P_{5/2}$	298 010.3	298 010.3 (0)	297 922.0 (88)	301 355.0 (−3345)
62	3s 3p 4p	(97)	$^4S_{3/2}$	299 369.3	299 369.3 (0)	299 406.0 (−37)	299 278.0 (91)
63	3s 3p 4p	(94)	$^2D_{3/2}$	301 109.8	301 109.8 (0)	301 065.0 (45)	304 748.0 (−3638)
64	3s 3p 4p	(94)	$^2D_{5/2}$	301 576.4	301 576.4 (0)	301 572.0 (4)	305 256.0 (−3680)

Table A1 *–continued.*

i	Conf.	Mixing (per cent)	LSJ	$E_{\rm exp}$	$E_{\rm NIST}$	$E_{\rm TEC}$	$E_{\rm t}$
65	$3p^2$ 3d	(57) +136(21) +186(c15 16)	$^2F_{5/2}$	–	–	307 653.0	310 103.0
66	$3p^2$ 3d	(58) +137(21) +187(c15 16)	$^2F_{7/2}$	–	–	308 001.0	310 451.0
67	3s 3p 4p	(94)	$^2S_{1/2}$	308 761.0	308 761.0 (0)	308 741.0 (20)	314 201.0 (−5440)
68	3s 3p 4s	(93)	$^2P_{1/2}$	308 939.3	308 939.3 (0)	308 913.0 (26)	313 410.0 (−4471)
69	3s 3p 4s	(93)	$^2P_{3/2}$	308 996.2	308 996.2 (0)	308 977.0 (19)	313 473.0 (−4477)

Notes. Energies in Kaysers. Only the lowest levels, corresponding to the 52 levels of Tayal's calculation are shown here (Tayal did not include the 3s 3p 4p levels). $E_{\rm exp}$: present experimental energies; $E_{\rm NIST}$: NIST experimental energies; $E_{\rm TEC}$ present calculation with TEC; $E_{\rm t}$: our ab-initio theoretical energies (without TECs). Values in brackets show differences with our experimental values.

The separation of the $3s^2$ 3p $^2P_{3/2,\,1/2}$ levels is obtained from measurements of the forbidden line in planetary nebulae; see e.g. Rank et al. (1970) and Feuchtgruber et al. (1997). We adopt the value of 951.4 kayser.

The 1–3 transition is blended with a much stronger O IV line, so the energy of level no. 3 (3s $3p^2$ $^4P_{1/2}$) is obtained from the 2–3 transition, for which we choose the 1423.885±0.005 Å wavelength, measured by Sandlin et al. (1986). We note that our HRTS measurement is 1423.84 Å, the same as the Kaufman & Martin (1993) value, while Young et al. (2011) report 1423.86±0.03 Å. Keenan et al. (2002) report instead a much lower value, 1423.79 Å. Our choice implies that the 1–3 transition should fall at 1404.85 Å. Ekberg & Åke Svensson (1970) identified this line, but reported a solar wavelength of 1404.77 Å, noting that this line is masked with the much stronger O IV line. The solar wavelength of the O IV line at 1404.77 Å was obtained from Burton & Ridgeley (1970), but the measurement was not very accurate. This wavelength was unfortunately later reported in following compilations, including Sandlin et al. (1986). We note that the wavelength of the O IV line as given by Sandlin et al. (1986) is 1404.82±0.01 Å, so it appears that the O IV and S IV lines are very close.

Level no. 4 (3s $3p^2$ $^4P_{3/2}$) produces a weak decay to the ground state, and a stronger 2–4 transition. We choose the Sandlin et al. (1986) measurement, 1416.928±0.005 Å, which implies that the decay to ground state should be at 1398.08 Å. We note that this decay was observed by Keenan et al. (2002) in the RR Tel spectrum, and that their STIS measurements (1398.044, 1416.872 Å) are relatively close, once a shift of 0.04 Å is applied.

The energy of level no. 5 (3s $3p^2$ $^4P_{5/2}$) is obtained from the 2–5 transition, observed at 1406.059±0.005 Å by Sandlin et al. (1986).

The energy of level no. 6 is obtained from the 1–6 and 2–6 transitions, observed at 1062.672 and 1073.522 Å by Bowen (1928). The energy of level no. 7 is obtained from the 2–7 transition, observed at 1072.992 Å by Bowen (1928).

The energy of level no. 8 is obtained from the 1–8 and 2–8 transitions, observed by Millikan & Bowen (1925) at 809.69 and 815.97 Å, respectively. The energy of level no. 9 is obtained from the 1–9 and 2–9 transitions, observed by Millikan & Bowen (1925) at 748.40 and 753.76 Å, respectively. The energy of level no. 10 is obtained from the 1–10 and 2–10 transitions, observed by Millikan & Bowen (1925) at 744.92 and 750.23 Å, respectively.

The energy of level no. 11 is obtained from the 1–11 657.34 Å line observed by Millikan & Bowen (1925). The energy of level no. 12 is obtained from the 2–12 661.42 Å line observed by Millikan & Bowen (1925). The energy of level no. 13 is obtained from the 1–13 551.17 Å line observed by Millikan & Bowen (1925).

The level no. 16 is quite important because there are three transitions, 3–16, 4–16 and 5–16, observed by Bowen (1928) at 798.265, 800.470 and 803.975 Å, that allow a consistency check of the relative energies of the three $^4P_{1/2}$ levels. We have indeed agreement within 1 kayser for the energy of level no. 16, assuming the Bowen (1928) measurements and our adopted energies for the $^4P_{1/2}$ levels. We note that such excellent agreement is not obtained with other choices of wavelength measurements.

The energy of level no. 21 is obtained from the 6–21 transition, observed at 852.716 Å by Bowen (1928).

Level 22 produces several weak lines. The strongest is the 7–22, observed by Bowen (1928) at 853.135 Å. We note a discrepancy in the energy obtained from the 9–22 transition, which should not be the line observed at 1286.063 Å, but the line observed at 1286.22 Å. The energies obtained from the 8–22 (1138.227 Å) and 10–22 (1296.64 Å) are in agreement within 3 kayser.

The energy of level no. 23 is obtained from the 6–23 transition, observed at 837.447 Å by Bowen (1928). The energy of level no. 24 is obtained from the 7–24 transition, observed at 836.286 Å by Bowen (1928).

Finally, the energies of the other levels are either slightly modified adopting the measurements reported by Kaufman & Martin (1993), or are left unaltered as they are in the NIST data base.

This paper has been typeset from a TEX/LATEX file prepared by the author.